Neutron spectroscopic factors of Ni isotopes

Jenny Lee, M.B. Tsang, W.G. Lynch
National Superconducting Cyclotron Laboratory, Department of Physics and Astronomy, and Joint Institute of Nuclear Astrophysics,
Michigan State University, East Lansing, Michigan 48824, USA
M. Horoi
Department of Physics, Central Michigan University, Mount Pleasant, Michigan 48859, USA
S.C. Su
Physics Department, Chinese University of Hong Kong, Shatin, Hong Kong, China

Abstract

The neutron spectroscopic factors for nickel isotopes have been extracted by performing a systematic analysis of the angular distributions measured from (d,p) transfer reactions. The results are compared to predictions of large-basis shell models with the GXPF1A interaction in the full fp model space, and the XT interaction in the ($f_{5/2}$, $p_{3/2}$, $p_{1/2}$, $g_{9/2}$) model space. For ground states, predicted spectroscopic factors using GXPF1A interaction with complete model space agree very well with experimental values. For excited states below 3.5 MeV, the agreement between data and shell model calculations with GXPF1A or XT interactions is not better than a factor of two. The level of disagreement is similar for both interactions except that the computation time is much faster using the XT interaction. Our work shows that the spectroscopic factors of Ni isotopes provide an independent test to shell model interactions in the pf model space.

The shell structure of the unstable doubly magic nucleus ^{56}Ni (N=Z=28) has attracted much attention recently. In most shell model calculations, the N=28 core in ^{48}Ca is assumed to be a well-established closed shell. However, Relativistic Hartree+Bogoliubov calculations predict a strong suppression of the N=28 shell gap for neutron rich nuclei [1]. While experimental investigations of the 2^+ energies of ^{36,38,40}Si provide evidence for the weakening of the N=28 shell gap in nuclei with large neutron excess [2], the evidence is inconclusive for the case of ^{47}Ar [3,4]. Recent measurements of the nuclear magnetic moment of the ground state of ^{57}Cu, which could be viewed as a valence proton outside a closed ^{56}Ni core, suggests significant breaking of the $f_{7/2}$ shell [5]. To further explore the property of the single particle states outside ^{56}Ni, we extracted the neutron spectroscopic factors, which measure the occupancy for the valence neutrons ranging from ^{57}Ni to ^{65}Ni isotopes. The extracted spectroscopic factors are important bench marks in evaluating different pf-shell model interactions that may be used to predict the structure of Ni or Cu nuclei, which are of special importance for the stellar evolution and electron capture in supernovae.

We extracted the neutron spectroscopic factors of ^{57,59,61,62,63,65}Ni isotopes, using the angular distributions measured in (d,p) reactions found in the literature[6-20]. We supplement these data sets with neutron ground state spectroscopic factors determined from ^{58,60,61,62}Ni(p,d) reactions [21-32] which should be the same as those determined from the inverse (d,p) reactions from detailed balance. To evaluate the effectiveness of the residual interactions and the model space used in the pf shell, these values will be compared to predictions from shell model calculations with two commonly used effective interactions and their associated model spaces.

In this work, we follow the conventional definition of an experimental spectroscopic factor, defined as the ratio of measured cross sections to the cross sections calculated with a reaction model. The reaction model used for the (p,d) and (d,p) reactions is the Johnson-Soper adiabatic three-body model that calculates the theoretical angular distributions [33] assuming unity spectroscopic factors. The Adiabatic Distorted Wave Approximation (ADWA) model takes into account the deuteron breakup in the mean field of the target. A priori, transfer reactions do not yield absolute spectroscopic

factors as the analysis depends on other input parameters such as the geometry of the bound state wave function as well as the optical potentials used in the reaction model [34-36]. However, if the analysis utilizes a consistent set of parameters, the relative spectroscopic factors could be determined reliably [36-38]. We choose the analysis approach of references [37, 38] as the spectroscopic factors obtained agree with the large-basis shell model predictions to ~20%, which are similar to the experimental uncertainties of the extracted spectroscopic factors [37,38]. In the reaction model calculations, the global nucleon-nucleus optical potentials in ref. [39] are adopted. The potential binding the transferred neutron to the core is chosen to have Woods-Saxon shape with fixed radius and diffuseness parameters, r_0=1.25 fm and a_0=0.65 fm. The depth of the central potential wells is adjusted to reproduce the experimental separation energies. All calculations make the local energy approximation (LEA) for finite range effects [40] using the zero-range strength (D_o^2=15006.25 MeV^2 fm^3) and range (β=0.7457 fm) parameters of the Reid soft-core $^3S_1$-$^3D_1$ neutron-proton interaction [41]. Nonlocality corrections with range parameters of 0.85 fm and 0.54 fm are included in the proton and deuteron channels [42]. We use the same source of input parameters for all the reactions analyzed here. The transfer reaction calculations are carried out using the code TWOFNR [43] which respects detailed balance between (p,d) and (d,p) reactions that connect the same states.

From the published angular distributions [6-32], which are of reasonable quality, we extracted about 180 spectroscopic factors for the Ni isotopes. These values are listed in Table I. Spectroscopic factors from the Evaluated Nuclear Structure Data File (ENSDF) compiled by the National Nuclear Data Center (NNDC) [44] are also listed in Table I in the last column. In general, the ENSDF values are taken directly from the published values, which came from different experiments and might be analyzed differently using different optical potentials and different reaction models. As a result, these SF values may not be consistent with each other or with the results from the present work. Fig. 1 compares the spectroscopic factors obtained in this work (y-abscissa) to those listed in ENDSF (x-abscissa). The solid line indicates perfect agreement. Most of the ENDSF values are about 30% larger than the values obtained in the present work. (The spectroscopic factors for the data set ^{61}Ni(d,p)^{62}Ni are not included in the comparison

because of the discrepancies between the ENSDF and published values in ref [21]. The second set of ENDSF values obtained from reference [45] for the same reaction does not have published angular distributions.)

Shell model calculations for Ni isotopes were available since 40 years ago. In the early calculations [46,47], ^{56}Ni is assumed to be an inert core and the influence of core excitation was taken into account in the effective residual interaction between the valence nucleons in the pf-shell. With advances in computational capability, many new effective interactions, which are the key elements for successful predictions, have been proposed. The GXPF1A interaction, a modified version of GXPF1 with five matrix elements, involving mostly the $p_{1/2}$ orbitals, has been adjusted to the experimental data [48]. Another interaction KB3G [49] has also been used to predict properties in the pf shell nuclei. The matching between the theoretical and experimental levels is based on the exact agreement of the quantum numbers (l,j) and spin-parity J^{π} of the transferred neutron and the approximate agreement of the energy of the states. In general, the agreement between energy levels is within 300 keV.

We first computed the neutron spectroscopic factors with GXPF1A and KB3G interactions using Oxbash, a large-basis shell model (LB-SM) code [50,51] with the truncated model space in which the $f_{7/2}$ orbital is completely filled by nucleons, without excitation. The comparison of the ground-state spectroscopic factors between experiments and truncated model space calculations are shown in the lower panels of Fig. 2. The ^{63}Ni nucleus is not included in the lower panels because the spin of the predicted ground state from both calculations is $5/2^-$ but the experimental value is $1/2^-$. Similarly, the ground state SF value of ^{61}Ni with spin of $3/2^-$ is not compared to the predicted value from GXPF1A calculation, which predicts $5/2^-$ for the ground state. When the ground states are matched in both calculations, the predicted spectroscopic factors are about 30% larger than the experimental values. The solid lines are the least square fits of the linear correlations between data and predictions. The slopes of the lines are labeled inside each panel. Figure 1 suggests that predictions from truncated model space are not reliable and we will not discuss results of calculations with truncated model space further.

We performed full pf model space calculations with interaction GXPF1A using the m-scheme code Antoine [52]. These calculations are CPU intensive. As the GXPF1 and KB3G interactions give similar results, we do not repeat such calculations with

KB3G interaction. Furthermore, it has been shown that with the improved modification in the monopole and pairing matrix elements of the Hamiltonian, the GXPF1A interaction is better than KB3G for the lighter isotopes around ^{56}Ni [53,54]. The predictions using GXPF1A interactions are listed in Table II. The ground state spectroscopic factors are plotted in the upper left panel of Fig. 2. Agreement with data is very good as indicated by the unity slope of the solid line which is the least square linear fit. This underscores the importance in using full model-space calculations.

In addition to the GXPF1A interactions, a new T=1 effective interaction for the $f_{5/2}$, $p_{3/2}$, $p_{1/2}$, $g_{9/2}$ model space has recently been obtained for the ^{56}Ni-^{78}Ni region by fitting the experimental data of Ni isotopes from A=57 to A=78 and N=50 isotones for ^{89}Cu to ^{100}Sn [55]. The interaction provides an improved Hamiltonian for Z=28 with a large model space and new Hamiltonian for N=50. It has been mainly used to describe heavier Ni isotopes using a ^{56}Ni core. The predictions from the XT interaction, using Oxbash code [51], are listed in Table II. The predicted ground state neutron spectroscopic factors are compared to the experimental values in the upper right panel of Fig. 2. The overall comparison suggests that the SF values predicted by the XT interactions are about 30% larger. Unlike the results from the truncated basis calculations, the predicted spins for all the ground states are correct.

Fig. 3 shows the ratios of the experimental SF values to predicted SF values as a function of the energy levels for all the states we can identify in shell model calculations with GXPF1A interaction (top panel) and with XT interaction (bottom panel). The solid lines (ratio=1) indicate perfect agreement between data and predicted results and the dashed lines above and below the solid lines indicate that data are $\pm$30% of the predicted values, respectively. In the current calculations with GXPF1A interaction, limited numbers of states mainly with excitation energy less than 3 MeV have been calculated because of the difficulties in identifying the states at high excitation energy and the CPU time required to do the calculations. Even though the XT interaction was developed to describe the heavy Ni isotopes around ^{67}Ni, predictions with the XT interactions are in reasonable agreement with experimental data for light mass Ni isotopes with A~60. Many more states are calculated and identified with the XT interaction than with the GXPF1A interaction. In Figure 3, the states, which are predicted by calculations using either the GXPF1A or XT interactions but not both, are represented by the symbols with

double edges. The current analysis yields spectroscopic factors that cluster around the large-basis shell model predictions similar to the excited states in the sd shell nuclei [56]. Aside from ground states (where the predictions by GXPF1A are better as shown in Fig. 2) and the light Ni isotopes (A<60), the scatter of the ratios in Figure 3 is similar in both calculations [57]. Since the discrepancy between the data and the predictions significantly exceeds the experimental uncertainties shown by the error bars (in the order of 30%), the inaccuracies in the predictions mainly reflect the ambiguities in the interactions used in the calculations.

More insights regarding the residual interactions may be obtained by combining the spectroscopic factors with energy level information. Fig. 4 plots the energy levels of ^{57,59,61,62,63,65}Ni nuclei where the lengths of the horizontal bars represent the values of the spectroscopic factors. Each panel compares the energy levels and SF values extracted from experiment to values obtained from shell model calculations for one isotope using the XT interaction. (Since only a few excited states have been obtained in the full fp model space with the GXPF1A interaction, these states are not plotted in Figure 4.) In the upper left panel of Figure 4, only two excited states in addition to the ground states have been measured for ^{57}Ni. The description by both calculations is quite reasonable. For the other Ni isotopes, shell model calculations tend to predict larger spectroscopic factors for the low-lying states, thus assigning larger single particle characteristics to these states. The number of unmatched levels increases with excitation energy. Above 3.5 MeV, we only have three states matched with predictions using the XT interactions. The ratios obtained for 4.709 MeV ($9/2^+$) and 5.429 MeV ($9/2^+$) states of the ^{59}Ni nucleus, and 3.686 MeV ($3/2^-$) state in ^{61}Ni are 7 and 3 and 17 respectively. The spectroscopic factors for all of them disagree with the shell model predictions beyond the systematics plotted in Figure 3. This suggests that properties of single particle energy levels at high excitation energy are not well described by the shell models even though the centroid of single particle energy may be determined from calculations especially when the hole states are taken into account [4].

In summary, neutron spectroscopic factors have been extracted for a range of Ni isotopes. The current set of measured spectroscopic factors provides an additional means other than energy spectra to test the shell model interactions in the fpg model space. The ground state neutron spectroscopic factors calculated with GXPF1A with full basis are in

better agreement with the data. For excited states of Ni isotopes beyond ^{60}Ni, the XT interaction predicts the spectroscopic properties of these nuclei reasonably well. It is advantageous to use XT interaction considering the ease in computation. Neither the GXPF1A nor the XT interaction gives good predictions of single particle states above 3.5 MeV. For the excited states below 3.5 MeV, the extracted spectroscopic factors cluster around the shell model values, but the agreement of the spectroscopic factors between data and calculations is not better than a factor of two. Since the experimental uncertainties are in the order of 20-30%, the large scatter of the data suggests that they can be used to evaluate newer interactions in the fpg model space. Until more accurate interactions become available for shell model calculations in the Ni region, it is currently not possible to determine if ^{56}Ni is a good double magic core for nearby isotopes by comparing experimental and predicted neutron spectroscopic factors.

Acknowledgement

The authors would like to thank Professor B.A. Brown and Professor J. Tostevin for fruitful discussions. This work is supported by the National Science Foundation under grants PHY-0606007, PHY 0216783 (JL, MBT, WGL) and PHY-0555366 (MH). Horoi acknowledges the NSF MRI grant PHY-0619407, which made possible the full fp model space shell model calculations with GXPF1A interaction. Su acknowledges the support of the Summer Undergraduate Research Experience (SURE) program sponsored by the Chinese University of Hong Kong.

References:

[1] G. A. Lalazissis *et al.*, Phys. Rev. C 60, 014310 (1999).

[2] C. Campbell et al., Phys. Rev. Lett. 97, 112501 (2006).

[3] L. Gaudefroy et al., Phys. Rev. Lett. 97, 092501 (2006).

[4] A. Signoracci and B. A. Brown, Phys. Rev. Lett. 99, 099201 (2007).

[5] K. Minamisono et al, Phys. Rev. Lett. 96, 102501 (2006).

[6] D. Sykes et al, Can. J. Phys. 50, 2096 (1972).

[7] E. Wesolowski et al., J. Phys. G 17, 955 (1991).

[8] I. M. Turkiewicz et al., Ncul. Phys. A143, 641(1970).

[9] T. R. Anfinsen et al., Ncul. Phys. A157, 561(1970).

[10] V. F. Litvin et al., Ncul. Phys. A 184, 105 (1972).

[11] M. S. Chowdhury et al., Ncul. Phys. A 205, 454 (1973).
[12] J. A. Aymar et al., Ncul. Phys. A 207, 596 (1973).
[13] J. A. Aymar et al., Ncul. Phys. A 213, 125 (1973).
[14] T. Taylor et al., Ncul. Phys. A 337, 389 (1980).
[15] O. Karban et al., Ncul. Phys. A 366, 68 (1981).
[16] K. Hatanaka et al., Ncul. Phys. A 419, 530 (1984).
[17] O. Iwamoto et al., Ncul. Phys. A 576, 387(1994).
[18] E. R. Cosman et al., Phys. Rev. 142, 673 (1966).
[19] E. R. Cosman et al., Phys. Rev. 163, 1134 (1967).
[20] K. E. Rehm et al., Phys. Rev. Lett. 80, 676 (1998).
[21] J. H. Polane et al., J. Phys. G15, 1715 (1989).
[22] H. Ohnuma et al., J. Phys. Soc. Jpn. 36, 1236 (1974).
[23] B. Mayer et al., Ncul. Phys. A 177, 205 (1971).
[24] F. M. Edwards et all., Ncul. Phys. A 199, 463 (1973).
[25] R. E. Anderson et al., Ncul. Phys. A 311, 93 (1978).
[26] K. Hosono et al., Ncul. Phys. A 343, 234 (1980).
[27] M. Matoba et al., Ncul. Phys. A 581, 21 (1995).
[28] J. C. Legg et al., Phys. Rev. 134, B752 (1964).
[29] R. Sherr et al., Phys. Rev. 139, B1272 (1965).
[30] D. H. Koang et al., Phys. Rev. C13, 1470 (1976).
[31] H. Nann et al., Phys. Rev. C28, 642 (1983).
[32] M. Matoba et al., Phys. Rev. C53, 1792 (1996).
[33] R.C. Johnson et al., Phys. Rev. C1, 976 (1970).
[34] N. Austen, Direct Nuclear Reaction Theories (Wiley, New York, 1970).
[35] G. R. Satchler, Direct Nuclear Reactions (Oxford University, Oxford, 1983).
[36] X. D. Liu et al., Phys. Rev. C69, 064313 (2004).
[37] M. B. Tsang, Jenny Lee and W. G. Lynch, Phys. Rev. Lett. 95, 222501(2005).
[38] Jenny Lee, M. B. Tsang and W. G. Lynch, Phys. Rev. C75, 064320 (2007).
[39] R. L. Varner et al., Phys. Rep. 201, 57 (1991).
[40] P. J. A. Buttle and L. J. B. Goldfarb, Proc. Phys. Soc. London 83, 701 (1964).
[41] L. D. Knutson, J. A. Thomson and H. O. Meyer, Ncul. Phys. A241, 36(1975).
[42] F. Perey and B. Buck, Nucl. Phys. 32, 353 (1632).

[43] M. Igarashi et al., Computer Program TWOFNR (University of Surrey version).

[44] http://www.nndc.bnl.gov/ensdf/

[45] R.H.Fulmer and A.L.McCarthy, Phys. Rev. 131, 2133 (1963)

[46] N. Auerbach, Phys. Rev 163, 1203 (1967).

[47] S. Cohen et al., Phys. Rev. 160, 903(1967).

[48] M. Honma, T. Otsuka, B.A. Brown and T. Mizusaki, Phys. Rev. C 65, 061301(R) (2002).

[49] A. Poves et al., Nucl. Phys. A694, 157 (2001).

[50] B. A. Brown and B. H. Wildenthal., Annu. Rev. Nucl. Part. Sci. 38, 29 (1988).

[51] B. A. Brown et al., Computer program, http://www.nscl.msu.edu/~brown/resources/resources.html.

[52] E. Caurier, shell model code ANTOINE, IRES, Strasbourg 1989-2004, E. Caurier and F. Nowacki, Acta Physica Polonica 30, 705 (1999).

[53] M. Honma, T. Otsuka, B.A. Brown and T. Mizusaki, Euro. Phys. Jour. A 25 Suppl.1, 499 (2005).

[54] M. Horoi et al., Phys. Rev. C 73, 061305(R) (2006).

[55] A. Lisetskiy et al., Phys. Rev. C 70, 044314 (2004).

[56] M.B. Tsang, Jenny Lee, S.C. Su, J.Y. Dai, M. Horoi, H. Liu, W.G. Lynch, S. Warren, NSCL preprint, MSUCL-1374(2008).

[57] Not plotted in Figure 3 is the 2.124 MeV ($1/2^-$) state in ^{61}Ni. The ratio of SF(MSU)/SF(XT) is 36, beyond the vertical scale in Figure 3. It is not clear why the discrepancy between experimental and shell model SF values is so large. The small predicted SF value for this state partly arises from the large SF values assigned to the $1/2^-$ levels at the lower energy.

Fig. 1. (Color online) Comparison of the extracted SF values in the present work and the compiled values in ENDSF [44]. The solid line indicates perfect agreement and dashed lines represent ±30% of solid line.

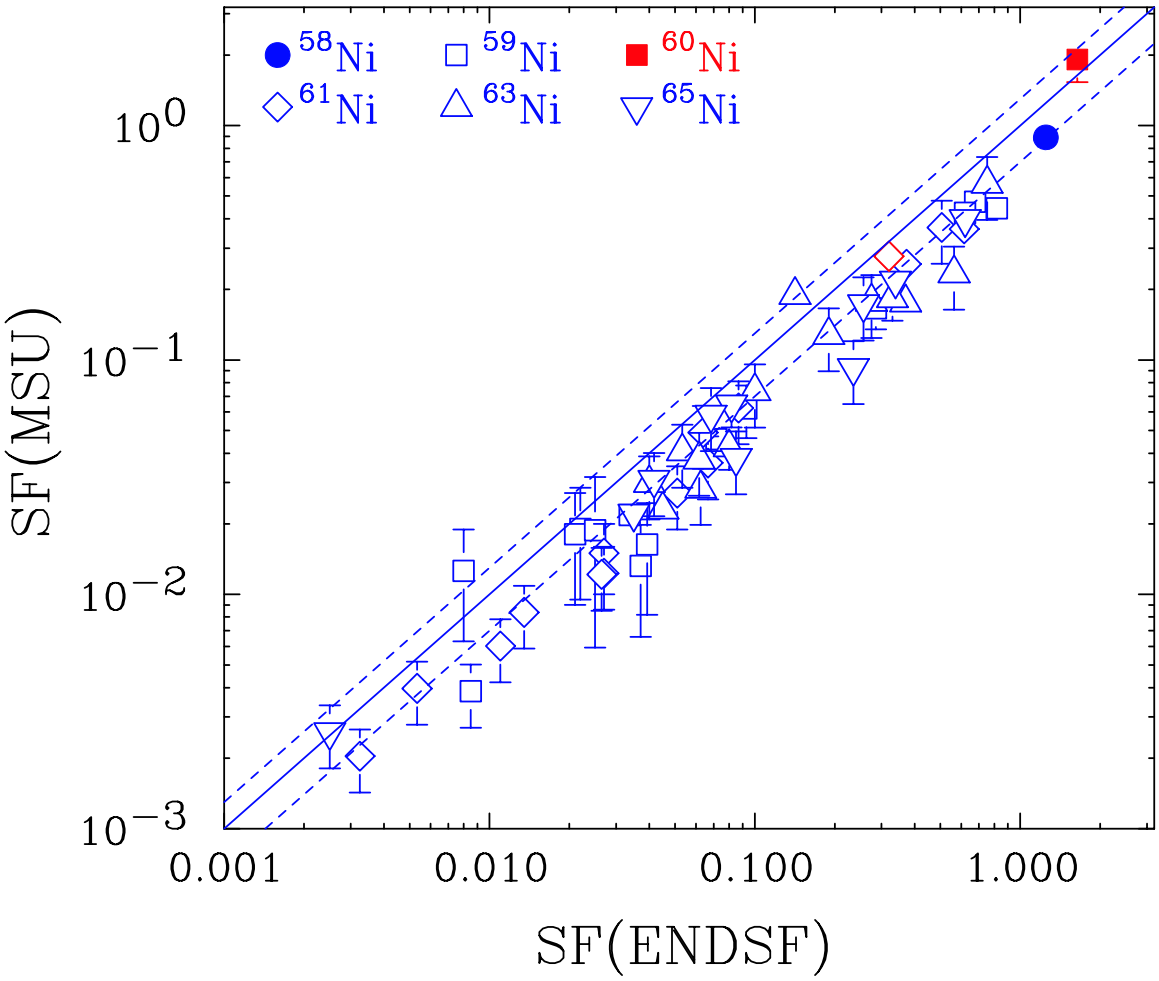

Fig. 2. (Color online) Comparison of the ground-state experimental SF values and the shell model calculations with GXPF1A interaction in pf model space, XT interaction in gfp model space and GXPF1A and KB3G interactions in the truncated pf model space. The solid lines are the linear fits with y-intercept fixed at zero. The slopes of the lines are listed in the individual panels.

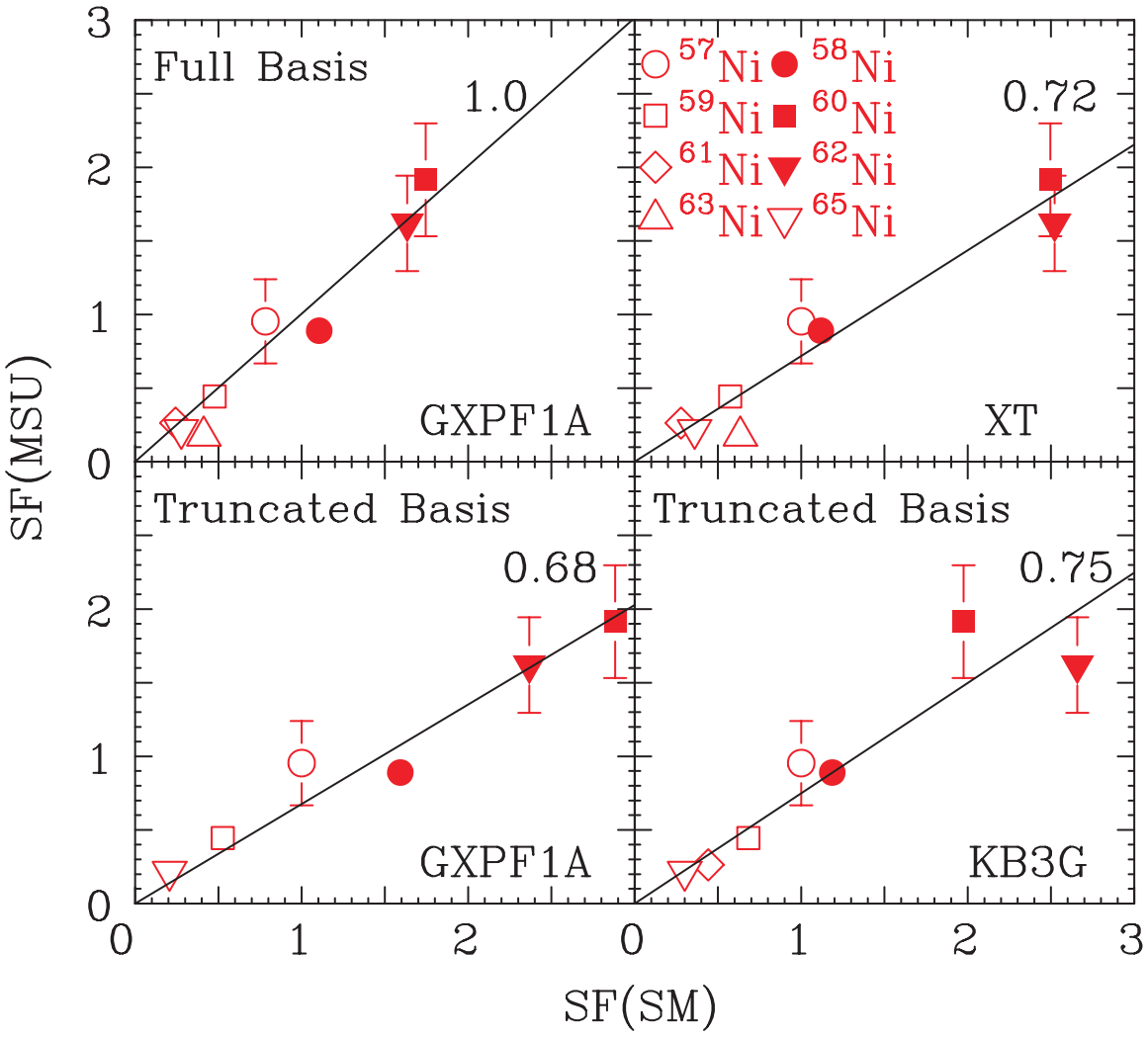

Fig. 3. (Color online) Ratios of the experimental SF values divided by values obtained from the shell model calculations with GXPF1A interaction in pf model space (top panel) and XT interaction in gfp model space (bottom panel). The solid line indicates perfect agreement and dashed lines represent ±30% of solid line.

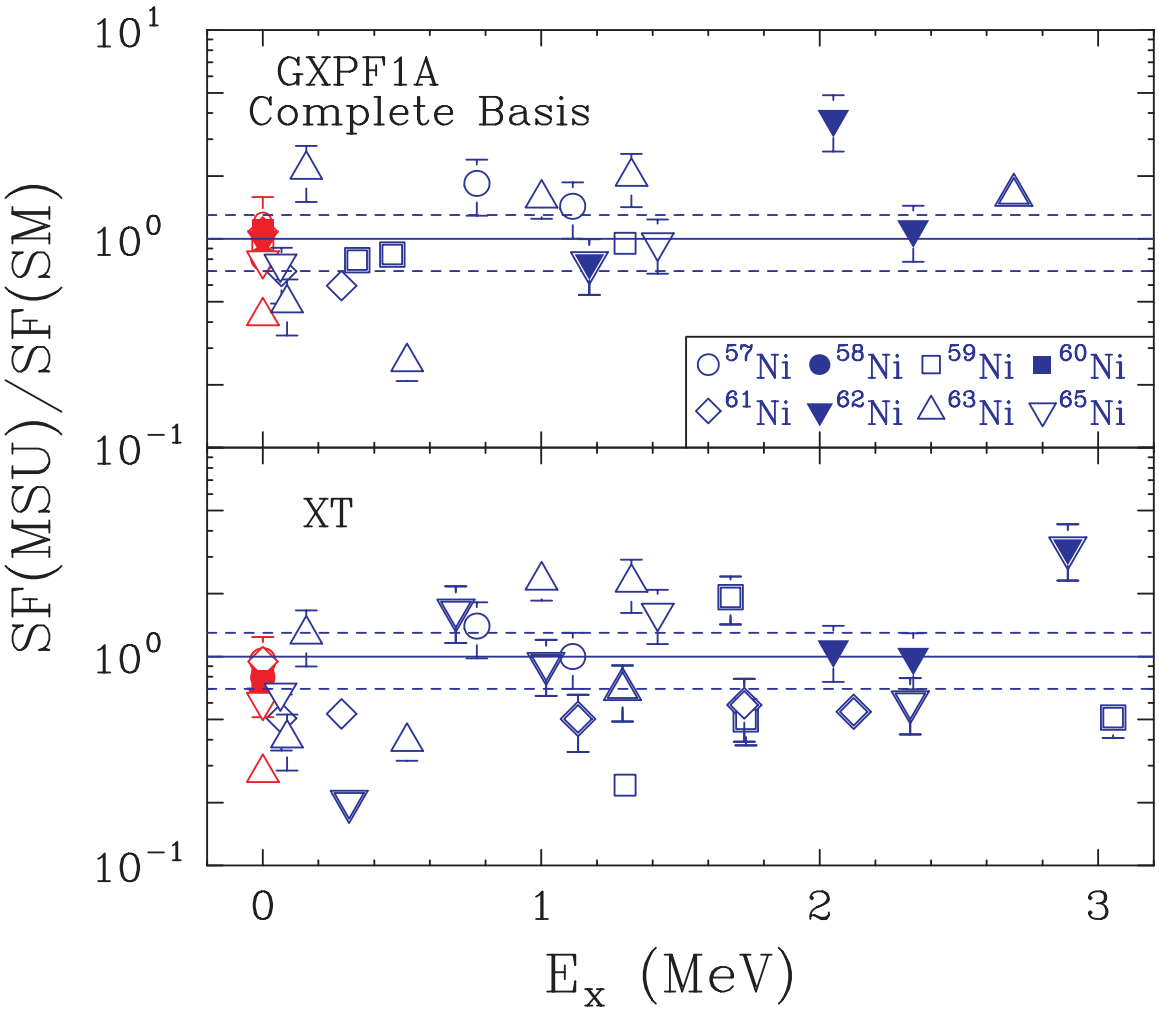

Fig. 4. (Color online) Plot of energy levels for ^{57,59,61,62,63,65}Ni nuclei with the length of the horizontal bars representing the values of the spectroscopic factors. The scale of the SF factor is given in the upper right corner in each panel.

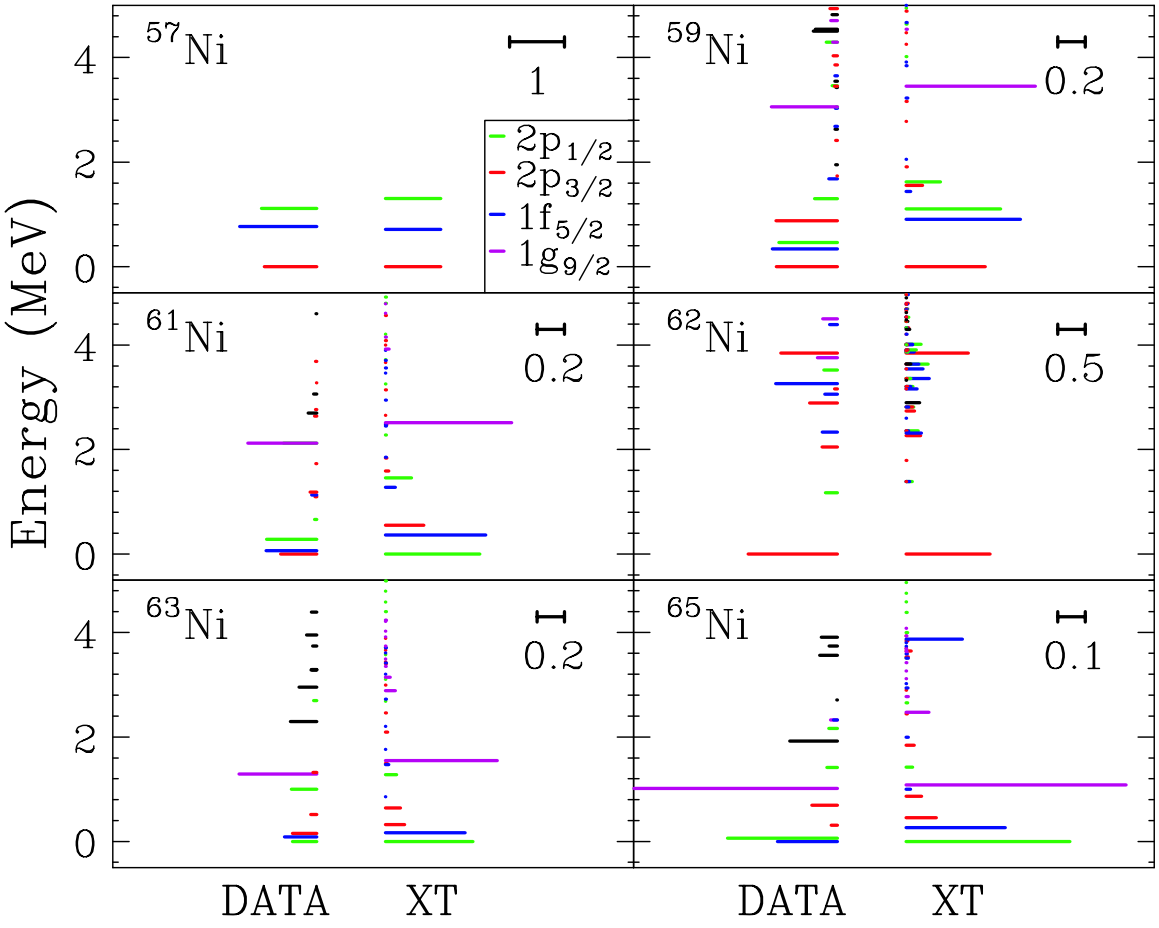

Table I. List of spectroscopic factors for the Ni isotopes. We adopt the energy levels compiled in the data base NUDAT by the National Nuclear Data Center [44]. SF(MSU) are SF values from the present work and SF(ENDSF) values are obtained from ENDSF data base [44]. Spin value, J, enclosed in "()" represents state with uncertain J value and the symbol "*" represents doublet state. State with undetermined parity (π) is labeled "N".

Nucleus	Ex (MeV)	l	J	π	SF(MSU)	Error	SF(ENDSF)
^{57}Ni	0.000	1	3/2	-	0.954	±0.286	
	0.769	3	5/2	-	1.400	±0.420	
	1.113	1	1/2	-	1.000	±0.300	
^{58}Ni	0.000	1	1.5	+	0.890	±0.087	1.250
^{59}Ni	0.000	1	3/2	-	0.444	±0.045	0.816
	0.339	3	5/2	-	0.472	±0.059	0.677
	0.465	1	1/2	-	0.424	±0.060	0.620
	0.878	1	3/2	-	0.046	±0.006	0.072
	1.301	1	1/2	-	0.166	±0.031	0.286
	1.680	3	5/2	-	0.062	±0.016	0.093
	1.735	1	3/2	-	0.004	±0.001	0.009
	1.948	3	7/2	-	0.013	±0.007	0.037
	2.415	1	3/2	-	0.013	±0.006	0.008
	2.627	3	7/2	-	0.016	±0.008	0.039
	2.640	1	(1/2)	-	0.022	±0.007	
	2.640	1	(3/2)	-	0.011	±0.003	
	2.681	3	(5/2)	-	0.019	±0.010	0.022
	3.026	1	1/2	-	0.023	±0.007	
	3.026	1	1/2*	-	0.009	±0.002	
	3.026	3	(5/2*)	N	0.016	±0.003	
	3.061	4	9/2	+	0.479	±0.096	
	3.429	0	(1/2)	N	0.010	±0.003	
	3.452	1	3/2	-	0.022	±0.003	0.034
	3.546	2	(5/2)	N	0.019	±0.006	
	3.652	3	(5/2)	N	0.018	±0.009	0.021
	3.858	1	3/2	-	0.019	±0.013	0.025
	4.036	1	(3/2)	-	0.031	±0.016	0.012
	4.506	2	5/2	+	0.175	±0.053	0.234
	4.542	2	5/2	-	0.161	±0.023	
	4.709	4	9/2	+	0.049	±0.024	0.098
	4.822	2	(5/2)	N	0.040	±0.020	
	4.939	1	(1/2)	N	0.054	±0.027	
	5.069	1	1/2	-	0.009	±0.003	0.017
	5.149	0	1/2	+	0.065	±0.019	0.093
	5.213	2	5/2	+	0.018	±0.005	0.026
	5.258	2	(5/2)	N	0.017	±0.009	

	5.429	4	(9/2)	+	0.080	±0.015	
	5.458	2	(5/2)	+	0.151	±0.075	
	5.528	0	1/2	+	0.120	±0.060	
	5.569	0	(1/2)	+	0.021	±0.006	0.024
	5.692	0	1/2	+	0.077	±0.023	0.126
	5.894	2	(5/2)	+	0.014	±0.004	
	6.142	1	1/2	-	0.027	±0.005	
	6.142	1	3/2	-	0.014	±0.003	
	6.206	2	(5/2)	+	0.023	±0.011	0.011
	6.284	2	(5/2)	N	0.053	±0.026	
	6.380	0	1/2	+	0.039	±0.012	0.078
	6.648	2	3/2	+	0.036	±0.011	
	6.648	2	5/2	+	0.024	±0.007	
	7.073	0	1/2*	+	0.027	±0.008	0.029
	7.073	2	5/2*	+	0.007	±0.002	0.012
	7.204	0	1/2*	+	0.017	±0.005	0.019
	7.204	2	5/2*	+	0.005	±0.001	0.012
	7.302	3	7/2	-	0.011	±0.003	0.017
	7.353	2	5/2	+	0.040	±0.020	0.007
	7.604	2	3/2	+	0.004	±0.001	
	7.604	2	5/2	+	0.013	±0.004	
^{60}Ni	0.000	1	3/2	-	1.915	±0.383	1.640
^{61}Ni	0.000	1	3/2	-	0.263	±0.026	0.346
	0.067	3	5/2	-	0.368	±0.110	0.507
	0.283	1	1/2	-	0.363	±0.051	0.615
	0.656	1	1/2	-	0.015	±0.005	0.027
	1.100	1	3/2	-	0.012	±0.004	0.027
	1.132	3	5/2	-	0.036	±0.011	0.067
	1.185	1	3/2	-	0.049	±0.015	0.064
	1.729	1	3/2	-	0.006	±0.002	0.011
	2.122	4	9/2	+	0.499	±0.071	
	2.124	1	1/2	-	0.242	±0.034	
	2.640	1	1/2	-	0.028	±0.009	
	2.640	1	3/2	-	0.014	±0.004	
	2.697	2	5/2	+	0.062	±0.019	0.087
	2.765	1	3/2	-	0.008	±0.003	0.014
	2.863	1	1/2	-	0.010	±0.003	
	2.863	1	3/2	-	0.005	±0.002	
	3.062	0	1/2	+	0.023	±0.007	
	3.273	1	(3/2)	-	0.002	±0.001	0.003
	3.382	1	1/2	-	0.007	±0.002	
	3.382	1	3/2	-	0.003	±0.001	
	3.506	2	3/2	+	0.158	±0.047	
	3.506	2	5/2	+	0.105	±0.031	
	3.686	1	(1/2)	-	0.018	±0.005	
	3.686	1	(3/2)	-	0.009	±0.003	
	4.568	2	(3/2)	+	0.006	±0.002	
	4.568	2	(5/2)	+	0.004	±0.001	

	4.600	2	5/2	-	0.004	±0.001	0.005
	5.112	1	1/2	-	0.035	±0.010	
	5.112	1	3/2	-	0.018	±0.005	
	5.185	0	1/2	+	0.027	±0.008	0.051
	5.309	0	1/2	+	0.012	±0.004	0.027
	5.723	2	(3/2)	N	0.055	±0.016	
	5.723	2	(5/2)	N	0.036	±0.011	
	5.987	0	1/2	+	0.021	±0.006	
	6.016	2	(3/2)	+	0.006	±0.002	
	6.016	2	(5/2)	+	0.004	±0.001	
	6.346	2	3/2	+	0.019	±0.006	
	6.346	2	5/2	+	0.013	±0.004	
	6.371	2	3/2	+	0.008	±0.002	
	6.371	2	5/2	+	0.006	±0.002	
	6.609	2	3/2	+	0.005	±0.002	
	6.609	2	5/2	+	0.004	±0.001	
^{62}Ni	0.000	1	0	+	1.619	±0.324	
	1.173	1	2	+	0.218	±0.065	
	2.049	1	0	+	0.280	±0.084	
	2.336	3	4	+	0.274	±0.082	
	2.891	1	0	+	0.505	±0.152	
	3.059	3	2	+	0.233	±0.070	
	3.158	1	2	+	0.052	±0.016	
	3.262	3	(2)	+	1.119	±0.336	
	3.370	1	1	+	0.295	±0.089	
	3.370	1	2	+	0.177	±0.053	
	3.519	1	2	+	0.248	±0.074	
	3.757	4	3	-	0.361	±0.108	
	3.849	1	0	+	1.028	±0.309	
	3.849	1	1	+	0.343	±0.103	
	3.849	1	2	+	0.206	±0.062	
	4.393	3	(2)	N	0.144	±0.043	
	4.503	4	(3)	-	0.264	±0.079	
	4.720	4	(3)	-	0.791	±0.237	
	4.863	4	5	-	1.079	±0.324	
	4.863	4	6	-	0.913	±0.274	
	5.331	2	(3)	-	0.163	±0.049	
	5.545	4	3	-	0.653	±0.196	
	5.545	4	4	-	0.508	±0.152	
	5.545	4	5	-	0.416	±0.125	
	5.545	4	6	-	0.352	±0.106	
	5.628	2	3	-	0.024	±0.007	
	6.103	2	1	-	0.451	±0.135	
	6.103	2	2	-	0.270	±0.081	
	6.103	2	3	-	0.193	±0.058	
	6.103	2	4	-	0.150	±0.045	
	6.540	2	1	-	0.350	±0.105	
	6.540	2	2	-	0.210	±0.063	

^{63}Ni	0.000	1	1/2	-	0.176	±0.025	0.370
	0.087	3	5/2	-	0.234	±0.070	0.563
	0.156	1	3/2	-	0.177	±0.053	0.275
	0.518	1	3/2	-	0.042	±0.008	0.080
	1.001	1	1/2	-	0.184	±0.037	0.330
	1.292	4	(9/2)	+	0.565	±0.169	0.750
	1.324	1	3/2	-	0.028	±0.008	0.063
	2.297	2	5/2	+	0.189	±0.027	0.142
	2.697	1	1/2	-	0.023	±0.003	0.045
	2.953	0	1/2	+	0.128	±0.038	0.190
	3.104	2	3/2	+	0.016	±0.005	
	3.104	2	5/2	+	0.011	±0.003	
	3.283	2	(5/2)	N	0.041	±0.012	0.053
	3.292	2	5/2	+	0.037	±0.011	
	3.740	2	(3/2)	N	0.030	±0.009	0.040
	3.951	2	5/2	+	0.074	±0.022	0.100
	4.387	2	5/2	+	0.038	±0.011	0.062
	4.622	2	3/2	+	0.053	±0.016	
	4.622	2	5/2	+	0.036	±0.005	
	5.060	2	(3/2)	+	0.009	±0.003	
	5.060	2	(5/2)	+	0.006	±0.002	
^{65}Ni	0.000	3	5/2	-	0.218	±0.031	0.338
	0.063	1	1/2	-	0.399	±0.056	0.620
	0.310	1	3/2	-	0.022	±0.003	0.035
	0.693	1	3/2	-	0.093	±0.028	0.235
	1.017	4	9/2	+	0.738	±0.221	0.085
	1.418	1	1/2	-	0.038	±0.011	0.257
	1.920	2	5/2	+	0.173	±0.052	
	2.163	1	(1/2)	N	0.031	±0.009	
	2.325	3	(5/2*)	N	0.030	±0.009	
	2.325	4	(9/2*)	N	0.050	±0.015	
	2.336	3	(5/2)	N	0.085	±0.025	
	2.336	3	(7/2)	N	0.063	±0.019	0.003
	2.712	2	3/2	+	0.003	±0.001	
	3.044	1	(1/2)	N	0.022	±0.007	
	3.044	1	(3/2)	N	0.011	±0.003	
	3.411	2	(3/2)	+	0.130	±0.039	
	3.411	2	(5/2)	+	0.087	±0.026	
	3.463	2	(3/2)	N	0.008	±0.002	
	3.463	2	(5/2)	N	0.005	±0.002	0.082
	3.563	2	5/2	+	0.065	±0.013	0.042
	3.743	2	5/2	+	0.031	±0.009	0.068
	3.907	2	5/2	+	0.058	±0.018	
	4.391	2	3/2	+	0.057	±0.017	
	4.391	2	5/2	+	0.038	±0.011	

Table II. Comparison of experimental and theoretical energy levels and spectroscopic factors for Ni isotopes.

				Ex (MeV)			SF			
Nucleus	l	J	P	NUDAT	GXPF1A	XT	MSU	Error	GXPF1A	XT
^{57}Ni	1	3/2	-	0	0	0	0.954	±0.286	0.783	1.000
	3	5/2	-	0.769	0.825	0.714	1.400	±0.42	0.76	1.000
	1	1/2	-	1.113	1.184	1.302	1.000	±0.3	0.698	1.000
^{58}Ni	1	3/2	-	0	0	0	0.890	±0.087	1.105	1.118
^{59}Ni	1	3/2	-	0	0	0	0.444	±0.045	0.477	0.574
	3	5/2	-	0.339	0.364		0.472	±0.059	0.597	
	1	1/2	-	0.465	0.595		0.424	±0.06	0.504	
	1	1/2	-	1.301	1.371	1.103	0.166	±0.031	0.175	0.685
	3	5/2	-	1.68		1.439	0.062	±0.016		0.032
	1	3/2	-	1.735		1.906	0.004	±0.001		0.008
	4	9/2	+	3.061		3.454	0.479	±0.096		0.938
	4	9/2	+	4.709		4.540	0.049	±0.024		0.007
	4	9/2	+	5.429		5.418	0.080	±0.015		0.028
^{60}Ni	1	3/2	-	0	0	0	1.915	±0.383	1.746	2.496
^{61}Ni	1	3/2	-	0	0	0.547	0.263	±0.026	0.244	0.278
	3	5/2	-	0.067	-0.006	0.364	0.368	±0.11	0.527	0.727
	1	1/2	-	0.283	-0.008	0	0.363	±0.051	0.609	0.683
	1	1/2	-	0.656		1.457	0.015	±0.005		0.188
	3	5/2	-	1.132		1.277	0.036	±0.011		0.072
	1	3/2	-	1.729		1.835	0.006	±0.002		0.010
	1	9/2	+	2.122		2.516	0.499	±0.071		0.917
	1	1/2	-	2.124		2.280	0.242	±0.034		0.007
	1	3/2	-	3.686		3.669	0.009	±0.003		0.001
^{62}Ni	1	3/2	-	0	0	0	1.619	±0.324	1.635	2.522
	1	1/2	-	1.173	1.148		0.218	±0.065	0.284	
	1	3/2	-	2.049	2.188	2.263	0.280	±0.084	0.075	0.259
	3	5/2	-	2.336	2.256	2.317	0.274	±0.082	0.247	0.275
	1	3/2	-	2.891		2.740	0.505	±0.152		0.153
^{63}Ni	1	1/2	-	0	0	0	0.176	±0.025	0.412	0.634
	3	5/2	-	0.087	0.158	0.171	0.234	±0.07	0.476	0.576
	1	3/2	-	0.156	0.373	0.319	0.177	±0.053	0.083	0.138
	1	3/2	-	0.518	0.77	0.643	0.042	±0.008	0.163	0.107
	1	1/2	-	1.001	1.216	1.282	0.184	±0.037	0.118	0.079
	1	9/2	+	1.292		1.546	0.565	±0.169		0.811
	1	3/2	-	1.324	1.363	1.491	0.028	±0.008	0.014	0.012
	1	1/2	-	2.697	2.79		0.023	±0.003	0.014	
^{65}Ni	3	5/2	-	0	0	0.264	0.218	±0.031	0.277	0.360
	1	1/2	-	0.063	0.025	0	0.399	±0.056	0.526	0.594
	1	3/2	-	0.310		0.453	0.022	±0.003		0.109
	1	3/2	-	0.693		0.864	0.093	±0.028		0.056
	1	9/2	+	1.017		1.082	0.738	±0.221		0.797
	1	1/2	-	1.418	1.100	1.425	0.038	±0.011	0.040	0.024
	2	9/2	+	2.325		2.474	0.05	±0.015		0.083